A thermal model to describe kinetic dispersion in rubber nanocomposites: The effect of mixing time on dispersion

Kabir Rishi[a,1], Vishak Narayanan[a,1], Gregory Beaucage[a,*], Alex McGlasson[a], Vikram Kuppa[b], Jan Ilavsky[c], Mindaugas Rackaitis[d]

[a] University of Cincinnati, Cincinnati, OH, 45242-0012, United States
[b] Nonstructural Materials Division, University of Dayton Research Institute, Dayton, OH, 45469, United States
[c] Advanced Photon Source, Argonne National Laboratory, Argonne, IL, 60439, United States
[d] Bridgestone Americas Center for Research and Technology, Akron, OH, 44301, United States

HIGHLIGHTS

- Ultra small-angle X-Ray scattering used to quantify nano-scale filler dispersion.
- Colloidal analogy relates temperature to time for mechanical mixing of nanofillers.
- van der Waals model used to estimate filler excluded volume and interaction energy.
- Excluded volume depends strongly on the size of nanofiller particles.
- Interaction energy depends on matrix viscosity and relates to filler wetting time.

ARTICLE INFO

ABSTRACT

Nanocomposites can be produced by a variety of processes. A common method used in industry is to mix a viscous polymer such as an elastomer compound, with nanofillers in a Brabender mixer or in a calendar. Dispersion has been quantified using a mixing index, *DR*, that is based on micrographs of reinforced elastomers on the micron-scale. A recently developed technique based on X-ray scattering allows for an alternative nano-scale description of dispersion based on a thermal-dispersion model where an analogy is made between temperature for thermal dispersion and nanocomposite processing conditions such as mixing time, mixing geometry, and viscosity for kinetic dispersion. In this paper the impact of mixing time on dispersion is investigated taking advantage of the van der Waals equation to describe excluded volume and interaction energy in the dispersion. It is found that the thermal-dispersion analogy is well behaved and can determine the wetting time for nano-scale incorporation of filler into elastomer. The nano-scale excluded volume depends only on the filler type and the excess excluded volume seems to be sensitive to the bound rubber layer. The pseudo-interaction energy is strongly dependent on viscosity and polymer chemistry. The thermal-dispersion model offers a novel approach to understanding kinetic dispersion in nanocomposites.

1. Introduction

Nano-reinforced elastomers have been an area of interest to the rubber industry for more than a century. These nanocomposites are widely used for applications such as tires and anti-vibration applications. Reinforcement requires good dispersion of the filler which is accomplished by mixing in an internal mixer or a two-roll mill. The dispersion of reinforcing nano-fillers such as carbon black and silica into an elastomeric matrix is of prime importance for the efficient use of raw materials and development of a product that possesses enhanced and tailored properties.

Mixing the various components that constitute a commercial tire is achieved by shear forces that distribute the fillers uniformly in the rubber matrix. This results in a "mixed-state" that encompasses the extent to which filler agglomerates break down to indivisible aggregates and their distribution throughout the rubber matrix. Both

---

* Corresponding author.
  E-mail address: gbeaucage@gmail.com (G. Beaucage).
  [1] Equal contribution by authors.

these processes occur simultaneously during the mixing process and a more fundamental understanding of the factors controlling them would help in improving the entire mixing operation.

The mixing process is highly convoluted and is comprised of various stages generally observed by the variation of mixing torque with mixing time [1,2]. Mastication of rubber involves the softening of the matrix by the application of heat and shear forces for suitable uptake of fillers. The initial stage is followed by filler incorporation in which the filler particles are wetted by the elastomer. This incorporation is generally associated with the observance of a peak in the mixing torque curve [3]. As the filler is incorporated into the rubber, the average agglomerate size of several microns decreases until it reaches a size scale where it cannot be broken down further under the application of shear forces. The smallest dispersible units in the range of a few hundred nanometers are aggregates, which can re-cluster into larger agglomerates due to weak van der Waals forces during the mixing process. The reduction in agglomerate size was described by Shiga and Furuta [4] using an "onion peel" model, where scanning electron microscopy (SEM) images revealed that aggregates peel off from the surface of the agglomerates in the manner that an onion would peel. Cotton [3] showed that the final stages of mixing are purely distributive in nature. Filler distribution can be enhanced by coupling agents that promote filler-polymer interactions. Raut et al. [5] used the block copolymer poly(butadiene-graft-pentafluorostyrene) as a coupling agent in styrene-butadiene rubber (SBR) carbon black nanocomposites to improve dispersion. The electron rich aromatic rings of carbon black had an affinity towards electron deficient pentafluorostyrene, whereas the butadiene backbone showed affinity towards SBR. Similarly, Mondal et al. [6] showed that in the presence of dispersing agents such as expanded graphite, carbon black-SBR nanocomposites showed a higher maximum torque value and exhibited greater bound rubber content in contrast to nanocomposites without graphite. It was concluded that expanded graphite led to improved polymer-filler interactions leading to better dispersion though the assessment of filler dispersion was only qualitative.

Macro-dispersion was first quantified by Leigh-Dugmore [7] through a series of micrographs that served as a tool for visual comparison. The dispersion rating based on the percentage of carbon black agglomerates below a certain size was revised by Medalia [8]. A model for the variation in the dispersion rating, $DR(t)$ with mixing time, t, was proposed by Coran and Donnet [9,10], equation (1). This model was related to the ratings assigned by Medalia [8]. It was considered that the amount of undispersed filler in the system was equal to the total number of agglomerates with an average size greater than 5 μm. This treatment was based on the flaw size of polybutadiene rubber, determined to be about 5 μm following Griffith's theory of crack propagation. A general improvement in properties was observed when the average size of the agglomerate population was less than 5 μm, which was associated with higher ratings. The Coran and Donnet function is given by,

$$DR(t) = DR_\infty - \frac{\alpha}{\exp(\beta t)} \tag{1}$$

where, $DR(t)$ has values between 0 and 10, with 10 indicating that the average size of all agglomerates is less than 5 μm. Since there is a possibility that the maximum value might never be observed, DR_∞ represents the rating at infinite time. α is a constant related to the amount of undispersed filler when dispersion commences; β, is an analogue to the specific rate in a first order chemical reaction. Hence, β would vary with material properties such as viscosity, mixing rate and temperature as well as mixing geometry. Since the dispersion process commences once all the filler particles have been incorporated into or wetted by the matrix, there exists a time delay, wetting time, before a dispersion rating can be assigned [11,12]. This characteristic time delay or filler incorporation time can be computed at $DR(t) = 0$. Current analysis of optical micrographs for assessment of macro-dispersion are based on the area ratio of agglomerates of a specific size [13,14].

Bohin et al. [15] proposed an alternative model, equation (2). Their dispersion model for carbon black under simple shear flow doesn't account for a delay for filler incorporation. In Bohin's model $DR(0) \approx 0$, can be assumed if the dispersion is modelled for the erosion of a single agglomerate. This means that the incorporation (or wetting) time for a single agglomerate is extremely small. The rate of agglomerate erosion was explained as a competition between the hydrodynamic shear force and the cohesive force that holds the agglomerate together. Bohin's model is given by,

$$DR(t) = \frac{10}{\left\{1 + \left(\frac{1}{\psi t}\right)\right\}} \tag{2}$$

where, the rate constant ψ, is directly related to the matrix viscosity and the shear rate. Yamada et al. [16] showed that increased matrix viscosity slowed matrix infiltration into the filler. A slower infiltration process at the same applied shear is associated with longer incorporation time indicating that the characteristic time delay would be longer if the matrix viscosity is higher.

Analysis of optical, SEM and TEM micrographs by numerical, statistical models and advanced computational geometry are popular methods of determining the extent of dispersion [17–26]. The strength and weaknesses of other dispersion characterization techniques has been reviewed [27]. Lively et al. [17] proposed a stereological approach where the diameter and size distribution of the agglomerates were estimated from optical micrograph images with smaller agglomerates indicating better dispersion. Khare et al. [18] provided a quantitative estimate of the degree of filler distribution by analyzing the size of regions in the composite that did not contain filler in TEM micrographs. For a well distributed system the size of the unfilled region was smaller as opposed to a poorly distributed system. Although, most image analysis techniques focus on developing a better statistical method to quantify dispersion, proper identification of the filler by image thresholding to completely eliminate the inhomogeneous background is generally overlooked as pointed out by Li et al. [19].

The extent of dispersion depends on the size scale of observation. Macro-dispersion involves the observation of a size-scale large enough to allow the averaging out of aspects such as structure and specific surface area of carbon black. Nano-dispersion involves observation on size scales comparable to the filler aggregate and primary particle. Jin et al. [28] showed that nano-dispersion depends linearly on primary particle size for carbon black in polybutadiene. Macro- and nano-dispersion may impact different mechanical properties of filled elastomers. Rishi et al. showed that nano-dispersion largely impacts the moderate to high-frequency dynamic response while macro-dispersion is important to static and low-frequency response [29]. It is useful to study the behavior of the indivisible aggregates (nano-dispersion) to understand the local dispersion of fillers and the impact on properties.

Several authors have characterized the compatibility of fillers in rubber matrices by investigating surface and aggregate structure. Stöckelhuber et al. [30] characterized filler-elastomer compatibility as a function of the surface energy and surface polarity of solid filler particles. It was proposed that the free energy of immersion, ΔG_i, could be represented as a function of the surface energies of the filler and the polymer-filler interface. This would reflect a thermodynamic contribution towards dispersion by quantifying the wettability of the filler particles by the polymer. This method however does not consider the contribution of the mechanical energy of mixing. Hassinger et al. [31] developed a quantitative tool to incorporate mechanical processing conditions in the prediction of interfacial thermodynamics. They proposed a set of descriptors that define the interfacial energy, the total power consumption and the volume fraction normalized filler surface area. The interfacial energy was based on the ratio of the work of adhesion between polymer-filler and filler-filler following Natarajan et al. [32] whereas, the normalized surface area was used to characterize the extent of dispersion based on TEM images. Using correlations between the three descriptors it was concluded that improved dispersion was

related to an increase in mixing energy.

Electrical conductivity (or inversely resistivity) measurements have also shown promising results in determining the extent of filler dispersion for carbon black-rubber nanocomposites [2]. Electrical conductivity is a function of filler grade as well as filler concentration. It increases with increasing filler in the nanocomposites until percolation. O'Farrell et al. [33] noticed an increase in volume resistivity with increasing mixing times for filler close to its percolation threshold. This meant that the number of direct contacts between the indivisible filler aggregates reduced with increasing mixing time indicating an improvement in dispersion. At longer mixing times, the appearance of a plateau in resistivity indicated a state of terminal dispersion such that the number of direct contacts remained unchanged. However, for fillers above percolation the change in volume resistivity was insignificant indicating that this measure of dispersion is suitable for dilute conditions i.e. in the absence of a percolated conductive network. Le et al. [34,35] performed online-conductivity measurements and showed that the variation in conductivity was proportional to mixing time. The change in conductivity which depends on the nano-filler contacts was related to the extent of dispersion. A peak in the measured conductivity close to the start of dispersion was associated with the filler incorporation time. This was found to be a function of the raw material characteristics such as the matrix viscosity and microstructure, as well as process parameters such as rotor speed and mixer configuration.

Jin et al. [28] considered a thermal-dispersion model for nano-dispersion. Clustering of colloidal particles in thermal equilibrium is opposed by the osmotic compressibility, $d\Pi/d\phi$, or the build-up of osmotic pressure, Π, with concentration, ϕ. Under dilute conditions, the osmotic pressure is estimated by the van't Hoff equation, $\Pi = \rho_{num}k_BT$. Like the ideal gas law, the equation doesn't account for binary interactions between filler aggregates and is unsuitable at larger particle concentrations, ρ_{num}, expressed in particles/cm^3. A virial expansion of osmotic pressure, defining the second virial coefficient, B_2, can describe deviations from ideality,

$$\Pi/k_BT = \rho_{num} + B_2\rho_{num}^2 + B_3\rho_{num}^3 + ... \tag{3}$$

where B_2, expressed in cm^3/particle, is the second virial coefficient and reflects deviations in osmotic pressure due to binary particle-particle interactions. The second virial coefficient, B_2, has been used to determine the stability of colloidal thermal dispersions [36]. For a stable colloid, with $B_2 > 0$, the dispersed phase remains evenly distributed throughout the solution, whereas particle clustering, sedimentation or flocculation occurs for unstable colloids with $B_2 < 0$. The power-series expansion in equation (3) can be modified by considering the mass density, ρ_M instead of number density of the particles [37] such that

$$\Pi/RT = \rho_M/M + A_2\rho_M^2 + A_3\rho_M^3 + ... \tag{4}$$

where, $\rho_M = (M/N_A)\rho_{num}$ is the concentration of colloidal particles in solution, M is the molar mass of a colloidal particle expressed as g/mol and N_A is the Avogadro's constant expressed in particles/mol. Here, $A_2 = (N_A/M^2)B_2$, such that $A_2 > 0$ favors particle dispersion whereas $A_2 < 0$ would indicate clustering, sedimentation or flocculation.

The above approach for thermally-dispersed mixtures has been extended to kinetically-dispersed binary filler-elastomer mixtures as reported by Jin et al. [28]. Jin reports on colloidal particles of carbon black or silica dispersed in a highly viscous elastomer phase. The high matrix viscosity limits the thermal motion of the particles since the particles do not significantly diffuse in the elastomer network. Consequently, the estimation of A_2 (or B_2) via osmometry is not possible. However, this can be overcome by estimating A_2 through ultra-small angle X-ray scattering (USAXS).

USAXS is used to characterize the structural hierarchy in filler particles under dilute conditions [38–40]. The particle morphology at each structural level can be fitted by the Unified Scattering Function

which is given as [41],

$$I_0(q) = \sum_0^n \left\{ G_i exp\left(\frac{-q^2R_{g,i}^2}{3}\right) + exp\left(\frac{-q^2R_{g,i+1}^2}{3}\right)B_i(q_i^*)^{-P_i} \right\} \tag{5}$$

where, "i" is an index for the structural level, lower values corresponding to smaller structures in a hierarchy. G and B are contrast factors such that G is proportional to the number density of particles at that structural level. R_g is the radius of gyration, q is the scattering or the reciprocal space vector, P_i is the fractal scaling for each structural level, "i". $q_i^* = q/\left(erf\left\{\frac{kqR_{g,i}}{\sqrt{6}}\right\}\right)^3$ where, erf is the error function and k is approximately equal to 1.06 for mass-fractal structures and 1 for solid particles that display an interface. The scattering vector is inversely related to the size scale under observation. Generally, four structural levels have been reported for carbon black [28,29]. Amongst this structural hierarchy, level 0 corresponds to graphitic layers, level 1 to primary particles, level 2 to intractable aggregates that are made up of fused primary particles. The aggregates are the smallest dispersible filler units in the elastomer. Finally, level 3 corresponds to agglomerated super-structures held by weak, van der Waals forces. Intermediate structural levels have also been reported by Koga et al. [42] for a certain grade of carbon black. The aggregate morphology can be specified by the degree of aggregation (z) or number of primary particles in an aggregate, the degree of branching, as well as polydispersity in z [43].

Fig. 1(a) is a representation of structural levels 1 and 2 for a filler particle under dilute conditions. However, loading levels used in the industry are usually above the overlap concentration in the semi-dilute regime. In this regime, aggregate features beyond a characteristic mesh size ξ, are obscured as shown in Fig. 1(b). For concentration normalized scattering intensity, this generally translates as a plateau in intensity, $I(q,\phi_v)/\phi_v$ at lower values (level 2) of the scattering vector q below a minimum $q^* \approx 2\pi/\xi$. An increase in filler concentration results in a decrease in this mesh size. At much lower q, however, the scattering intensity shoots up owing to agglomerated super-structures that are comprised of fused aggregates in 3-D domains or mass fractal networks [28]. This macro network is in dilute conditions until about 20 vol percent filler well above the nanoscale overlap concentration observed
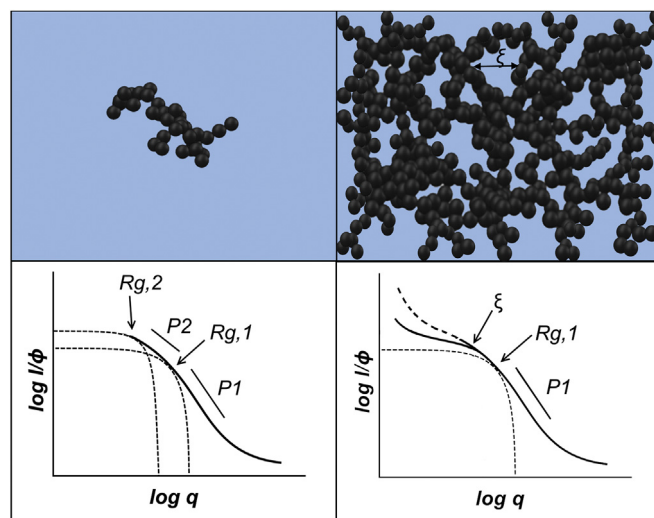
Fig. 1. (a) Cartoon of smallest dispersible unit (filler aggregate) with the corresponding scattering curve under dilute conditions. The filler exhibits a hierarchical structure and the scattering curve resolves each structural level as a power law slope (P_1, P_2) that gives information about the shape and a knee region that provides the size ($R_{g,1}$, $R_{g,2}$) of that level. (b) Cartoon indicating filler aggregate screening characterized by loss of structural resolution at large sizes for high concentrations, the corresponding scattering curve translates this loss in structural features as loss of reduced intensity at the aggregate level compared to the dilute scattering profile.

in scattering. This discrepancy in percolation volume fraction for the two networks and the hierarchical structure are caused by the innate immiscibility of carbon black in elastomer which causes local nano-scale clustering and percolation in domains of the nanostructure at concentrations around 5 vol percent. For this reason, the effect of screening in the present case is restricted to the primary particle and the aggregate level. The extent of screening is quantified in analogy to thermally dispersed colloidal systems using the random phase approximation [44] such that,

$$\left(\frac{I(q, \phi_v)}{\phi_v}\right)^{-1} = \left(\frac{I_0(q, \phi_0)}{\phi_0}\right)^{-1} + \nu\phi_v \tag{6}$$

where, ν is the screening parameter that quantifies the extent of structural overlap at large sizes. ν is expressed in cm and is a constant for a filler-elastomer combination under a set processing time. ϕ_v is the filler volume fraction, $\frac{I(q, \phi_v)}{\phi_v}$ is the volume fraction normalized scattering intensity; whereas, $\frac{I_0(q, \phi_{v,0})}{\phi_{v,0}}$ is the normalized intensity for the filler under dilute conditions below the nanoscale overlap concentration, in cm^{-1}. The screening parameter, ν, is related to A_2 by

$$A_2 = \frac{\nu\langle\Delta\rho^2\rangle}{2N_A\rho_f^2} \tag{7}$$

where, $\langle\Delta\rho^2\rangle$ is the square of the difference in scattering length density between the filler and elastomer expressed in cm^{-4} which is a measure of contrast, and ρ_f is the filler density [28]. In this case A_2 is a pseudo-second virial coefficient since the system is not thermally controlled but in analogy is dispersed by accumulated shear strain and is expressed in $mol\ cm^3/g^2$.

In colloidal mixtures, such as polymer solutions, printing inks, milk, red blood cells etc., dispersion of the particles is caused by thermally-driven, Brownian motion associated with k_BT that displays true thermodynamic behavior. In such cases, the dispersed nanoparticles might be separated by amplifying gravity or a settling force in a centrifuge to overcome k_BT. These thermally-dispersed colloids generally have a favorable surface interaction with the matrix, that is, they are stabilized by a surfactant or have a natural interfacial compatibility. These systems do not flocculate, sediment or cluster under normal conditions. On the other hand, mechanically-dispersed colloids exist in a kinetically locked-in state. The nanoparticles in such systems would normally flocculate, settle or cluster except for the action of mechanical dispersion coupled with a viscous, glassy, or semi-crystalline matrix phase. Carbon or silica nanofillers in an elastomer are examples of kinetically-dispersed colloids. In these cases, the properties are tied to the poor interfacial compatibility between the dispersed phase and the matrix phase coupled with the processing history leading to a more complex dispersed structure which may have serendipitous advantages compared with thermally-dispersed colloids.

In kinetically-dispersed colloids spontaneous diffusion of colloidal particles can occur [45], depending on the experimental conditions and given sufficient residence time, after or in conjunction with processing. Often, this thermal diffusion favors clustering on the nanoscale rather than dispersion leading to potential control of a complex, hierarchical nano-to macro-scale structure. However, the dispersion of nanofillers in a highly viscous elastomer, such as in industrial tires, is expected to be dominated by mechanical mixing. During mechanical mixing, the shear forces acting on weak agglomerates break and disperse the filler aggregates. These dispersible filler aggregates can re-cluster into agglomerates due to high surface energy.

Forces applied in mechanical mixing are amplified unevenly at different size scales following the lever rule leading to a "top-down" dispersion compared with the "bottom-up" dispersion in thermally-dispersed colloids. Clustering of filler particles to percolated nanofiller clusters, on the nanoscale is opposed by the application of mixing energy. Mixing energy has a smaller impact on the nanoscale since the lever arm is much smaller. On a larger length scale thermal transport is

insignificant and the lever arm for mixing is much larger, thus mechanical mixing leads to dispersion on large and intermediate length scales. At sufficient concentration kinetically-dispersed nanoclusters can percolate on a micron length-scale. This micron-scale network of nanoscale clusters has been observed by TEM, X-ray tomography, and by optical techniques.

The structural model proposed in this paper involves a dilute structure composed of aggregates of primary particles which are dealt with as rigid structures not impacted by kinetic or thermal dispersion. The structural model assumes that these intransigent aggregates cluster on the nano-scale forming a nano-network at about 5 vol percent which is responsible for much of the dynamic response; and these clusters of aggregates further percolate to form a micron-scale network at about 20 vol percent which is responsible for the low-frequency response and features such as the Payne effect. The final nanocomposite is a complex hierarchy of two percolated networks associated with immiscibility on the nanoscale and dispersion on the micron-scale.

Filler dispersion in elastomers is generally achieved by mechanical mixing under high shear conditions. Dispersion is subject to various controls such as processing time, viscosity, temperature (which impacts viscosity), and shear rate, as discussed earlier. An estimation of A_2 as a function of mixing time is a suitable approach to quantify nano-dispersion of filler aggregates with larger values of A_2 indicating better dispersion. Also, using the analogy between dispersion in thermally-dispersed, colloidal mixtures and the kinetics of mixing in filled elastomers, as discussed above, an approximate equivalence can be proposed between mixing time and temperature as they impact dispersion as shown in Fig. 2. This is because mixing time increases the accumulated strain in the sample leading to greater dispersion similar to the effect of temperature on diffusive distribution in a thermally-controlled colloidal system. This analogy has limitations due to the inhomogeneity of accumulated strain in a mixer compared to thermal motion.

The temperature dependence of the second virial coefficient, B_2, for thermally-dispersed, colloidal solutions can be obtained by describing the second virial coefficient of osmotic pressure, equation (3) with the van der Waals equation of state, such that

$$B_2(T) = b - \frac{a}{RT} \tag{8}$$

where, b is the volume correction term due to the excluded volume of the colloidal particles and a is the pressure correction term associated with inter-particle attraction. B_2 is related to A_2 by the molar mass of the particle, $A_2 = \left(\frac{N_A}{M^2}\right)B_2$ as discussed previously. For mechanically-mixed, kinetically-dispersed filler-elastomer nanocomposites, A_2 could be expressed as a function of mixing time, t, in direct analogy to equation (8), considering that the mechanical mixing energy is a direct function of the mixing time at a constant strain rate. Thus,
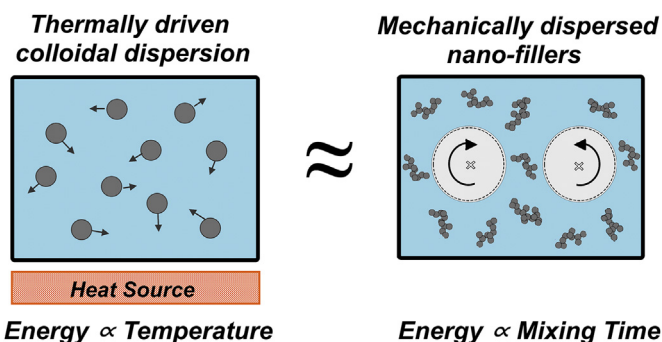
Fig. 2. A cartoon depicting the thermally-dispersed, colloidal analogy for mechanically mixed rubber-carbon black nanocomposites. The figure on the left shows colloidal particles in a solution where the average energy possessed by the particles is proportional to the temperature, T of the medium. The figure on the right shows carbon black aggregates in a rubber medium. The average kinetic energy is proportional to the total mixing time, t.

$$A_2(t) = \frac{N_A}{M^2}\left(b^* - \frac{a^*}{t}\right) \tag{9}$$

where, b^* and a^* are analogues to b and a for thermally-dispersed, colloidal particles in equation (8). $M = zN_A\rho_f\left(\frac{\pi d_p^3}{6}\right)$ is the molar mass expressed in g/mol which depends on the Sauter mean diameter of the primary particle, d_p and the degree of aggregation, z. The excluded volume, b^*, that dominates inter-particle repulsion is expected to be dependent on the size of the filler particle. However, a^*, which governs the inter-particle attraction would be affected by matrix viscosity as well as the accumulated shear during the mixing process. Following equation (9), A_2 should increase with mixing time and plateau at infinite mixing time thus agreeing with the results based on macro-dispersion studies [10,12]. Since dispersion as a function of mixing time is associated with positive values of A_2, a critical time, t^* can be defined when $A_2 = 0$ at $t^* = \frac{a^*}{b^*}$. This is expected to be related to the filler incorporation or wetting time as discussed in the case of macro dispersion per equation (1).

In this paper, A_2 is computed as a function of mixing time for elastomer/carbon black systems with variable melt viscosity and elastomer type. The dependence of the pseudo-van der Waals constants, a^* and b^* on elastomer and filler properties is discussed. A link is established between the macro dispersion characterization used in industry and the nano dispersion characterization proposed here. The description of nano-dispersion through the screening parameter, ν, proposed in this study, is expected to impact dynamic mechanical properties at low strain amplitude as recently reported [27]. This parameter could also correlate to other mechanical properties such as tensile strength, rebound resilience and tear strength of the nanocomposite, although this would be the subject of a future study. Additionally, the pseudo-interaction term, A_2, can be used to generate a potential for input to course-grained simulations for filler mixing in elastomers.

2. Experimental

Table 1 lists the elastomers used to prepare nanocomposites. Butadiene and styrene-butadiene rubbers are designated as B and SB respectively. The suffix for each polybutadiene rubber grade indicates the Mooney viscosity (B38 has a Mooney viscosity of 38 M. U.). The suffix for each styrene-butadiene rubber grade indicates the Mooney viscosity followed by the styrene content in the grade (SB80-38 has a Mooney viscosity of 80 M. U. and 38 wt percent styrene content). Note that the cis, trans and vinyl content of all butadiene rubbers are the same. Two grades of carbon black filler were provided by Cabot Corporation, 1095 Windward Ridge Parkway, Suite 200 Alpharetta, GA 30005. The commercial carbon blacks VULCAN 8 and VULCAN 3 conformed to ASTM N110 and ASTM N330 values respectively. The specific surface areas of N110 and N330 carbon blacks, 123 m^2/g and 76 m^2/g respectively, were obtained from the product data sheets [46]. The density of both carbon blacks was 1.9 g/cm^3. An antioxidant and antiozonant, 6PPD (N-(1,3-dimethylbutyl)-N'-phenyl-1,4-phenylenediamine), used during compounding, was provided by TCI America, 121 Domorah Drive, Montgomeryville, PA 18936. No crosslinking agents were used.

Mixing of carbon black and elastomer was accomplished in a 50g

Brabender mixer equipped with two rotor speeds of 30 and 60 rpm. The rubber was initially charged into the mixer at 30 rpm and the clock was started when the system equilibrated to the set temperature of 130 °C. The antioxidant was charged after 30s. Once the time reached a minute carbon black was added. The time for carbon black addition was also 30s following which the mixer speed was increased to 60 rpm. The nanocomposite was discharged following thorough mixing at times viz. 6, 8, 12, 18 and 24 min. The carbon content in the prepared samples for each mixing time was 1 (dilute), 5, 15 and 30 wt percent. The melt temperature during mixing was controlled by forced air and varied between 130 ± 4 °C.

For scattering studies, the processed elastomers were pressed into a washer such that a consistent thickness of 1.2 mm was maintained. These clamped specimens were subsequently baked in an oven at 100 °C for 10 min to ensure uniform thickness. USAXS measurements were taken at three positions within each sample. The three measurements made at different positions in the mixed sample are averaged and the concentration series is used to determine an average A_2. Despite the expected inhomogeneity in the mechanically mixed samples, a great difference in the three measured values for any of the mixing times was not observed. Measurements were performed at the Advanced Photon Source, Argonne National Laboratory using the ultra-small-angle X-ray scattering (USAXS) facility located at the 9 ID beam line, station C. All USAXS data was corrected for background and desmeared. This instrument is designed and operated by Jan Ilavsky [47].

For microscopy studies, thin sections of about 80 nm were sliced from the nanocomposites using a cryo-ultramicrotome at temperatures below the glass transition temperature of the matrix. The thin sections were collected on 200-mesh carbon-coated copper support grids. STEM micrographs were obtained from a transmission electron microscope with an accelerating voltage of 25 kV and an emission current of 10 microamps.

3. Results

3.1. Characterizing the dispersed filler particles

Carbon black is a hierarchical filler material that displays different structural levels which build upon each other. For this analysis, only the primary particle and aggregate levels are considered. This structural hierarchy is elucidated in combined small angle x-ray and ultra small angle x-ray scattering measurements (SAXS and USAXS) where the reciprocal lattice vector varies between 0.0001 and 1 Å^{-1}. Fig. 3 shows a log-log plot of the volume fraction normalized intensity as a function of reciprocal space vector $\left(\frac{I_0(q, \phi_{v,0})}{\phi_v} \text{ vs.} q\right)$ for dilute (0.5 vol percent) B45-N110 nanocomposites processed at different mixing times. The scattering curves are analyzed by first subtracting the scattering profile of the pure rubber from that of the composite, and then normalizing by the volume fraction. Each level is characterized by a Guinier region (Gaussian decay) followed by a power-law regime in q. It is observed that the scattering profiles, in the q-range indicated by dashed vertical lines in Fig. 3, are independent of mixing time.

Agglomerates comprising many aggregates are often observed by a

Table 1
Rubber grades and properties. Grades have been designated to provide information on viscosity and chemical structure (B38 has a Mooney viscosity of 38 M. U. and SB80-38 has a Mooney viscosity of 80 M. U. and 38% styrene content).

Elastomer	Grade	% cis	% trans	% vinyl	% styrene	Density (g/cc)	Mooney Viscosity (M.U.)
Polybutadiene rubber	B38	38	51	11	–	0.9	38
	B45	38	51	11	–	0.9	45
	B54	38	51	11	–	0.9	54
Styrene-butadiene rubber	SB80-38	–	–	24	38	0.96	80
	SB50-38	–	–	25	38	0.96	50
	SB50-26	–	–	44.5	26	0.94	50
	SB62-26	–	–	44.5	26	0.94	62

Fig. 3. Dilute USAXS curves for 0.5 vol percent B45-N110 nanocomposites milled at different processing times. The q-range between the dashed lines used to analyze the carbon black structure corresponds to level 1 (primary particle) and level 2 (aggregate) of the structural hierarchy; USAXS curves for dilute (0.5 vol percent) B45-N330 nanocomposites are shown in Fig. S1 in the supplemental material.

power-law at the lowest-q. The agglomerate level is not considered in fits for the virial coefficient since the agglomerates are associated with the macrostructure rather than the nanostructure. A two-level Unified Function, equation (5), is fit to the region lying between the dashed lines as indicated in Fig. 3 that includes level 1 (primary particle) and level 2 (aggregate). The high-q regime, between 0.008 and 0.025 Å^{-1}, pertaining to primary particle, is fit to a power-law slope of -4 (P_1) allowing calculation of the Sauter mean diameter, $d_p = \frac{6}{\left(S/V\right)}$. A power-law slope of -4 is a signature of scattering from a smooth and sharp surface. This characteristic surface fractal scaling usually varies between -3.7 and -4 in the q-range considered, thus validating the assumption [42,48]. The corresponding radius of gyration of the primary particle is 33 ± 1 nm. The aggregate is characterized in the mid-q region between 0.0008 and 0.008 Å^{-1} by a weak power-law that shows mass fractal scaling with a slope of about $P_2 = -2.2$ ($d_f = 2.2$).

The fit parameters for each of the dilute (0.5 vol percent) N110 and N330 carbon black based nanocomposites at different mixing times are listed in Table S1 and Table S2 respectively in the supplemental material. For a given nanocomposite the average size of the aggregates ($R_{g,2}$) and that of the primary particles ($R_{g,1}$) remain consistent within experimental error over the duration of mixing. The same is observed for the average aggregate structure which shows a consistent mass-fractal scaling, d_f, over the mixing operation. The mixing conditions thus show no effect on the average local structures under dilute conditions. This is unlike macro-dispersion which is modelled by a reduction in agglomerate size [15] as followed by visual comparison with micrographs [9,10]. This result indicates that any changes in local structure with mixing time are purely distributive in nature as discussed in the following sections.

The fit parameter, B_1, provided in Table S1 and Table S2 in the supplemental material is related to the surface area to volume ratio, $\left(S/V\right)$ from which the diameter of an equivalent sphere (Sauter mean diameter), $d_P = \frac{6}{\left(S/V\right)}$, of the primary particles can be calculated.

Table 2
Parameters calculated for dilute scattering curves for B45-N110 and B45-N330 nanocomposites from the obtained scattering parameters in Table S1 and Table S2 in the supplemental material. The calculated parameters for SB50-26-N110 and SB50-26-N110 are listed in Table S3 in the supplemental material.

Nano composite	Mixing time (mins.)	d_p (nm)	z	R_{eted} (nm)
B45-N110	6	29 ± 1	20 ± 3	105 ± 14
	8	28 ± 1	24 ± 5	110 ± 12
	12	29 ± 1	16 ± 3	94 ± 9
	18	28 ± 1	12 ± 1	81 ± 8
	24	30 ± 1	21 ± 6	125 ± 24
B45-N330	6	44 ± 1	9 ± 4	108 ± 22
	8	46 ± 1	8 ± 4	106 ± 23
	12	45 ± 1	7 ± 3	94 ± 15
	18	45 ± 1	7 ± 3	94 ± 18
	24	46 ± 1	6 ± 1	86 ± 6

Additionally, the number of primary particles within an aggregate is specified by the degree of aggregation, $z = \left(G_2/G_1\right) + 1$ [28,43]. The end-to-end distance of the aggregate is related to d_p, z and d_f, the mass fractal dimension of the aggregate by, $R_{eted} = d_p(z)^{1/d_f}$. Table 2 lists these calculated parameters at different mixing times for B45-N110 and B45-N330 nanocomposites. The primary particle diameter, $d_{SSA}(nm) = \frac{6000}{\rho_f SSA}$, is generally calculated from the specific surface area [49] measured in m^2/g and the filler density in g/cm^3. d_p for N110 is about 29 ± 1 nm which agrees with d_{SSA} of about 26 nm, whereas d_p for N330 is about 45 ± 1 nm which agrees with d_{SSA} of about 42 nm. The number of primary particles in an N110 aggregate is larger than that for an N330 aggregate. This is expected since $d_p^{N110} < d_p^{N330}$, and consequently the surface area is greater leading to greater aggregation.

Fig. 4 shows a TEM image of a dilute (0.5 vol percent) B45-N110 nanocomposite that was mixed for 24 min. The chain-like structures indicated in Fig. 4 (a) and (b) are the dispersed filler aggregates with an average size of about 150 nm. This agrees well with the aggregate end-to-end distance, R_{eted} obtained from scattering studies listed in Table 2. Particles were simulated using monomer-cluster growth with the degree of aggregation, $z = 21$, from scattering results and varying the sticking probability until the fractal dimension $d_f \sim 2.1$, the minimum
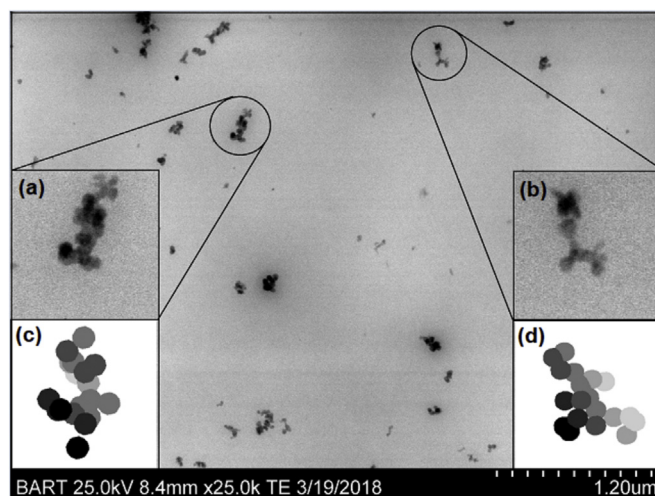
Fig. 4. TEM image of 0.5 vol percent B45-N110 nanocomposite processed for 24 min. Under dilute conditions, there is no overlap of structural features and individual aggregates can be isolated. (a–b) These aggregates are about 150 nm in size which is approximately the same as the R_{eted} of the aggregate based on fits to the scattering curves. The end-to-end distance of the aggregate is related to d_p, z and d_f as $R_{eted} = d_p(z)^{1/d_f}$; (c–d) Simulated N110 aggregates based on the scattering fit results comprising of 21 primary particles using Mulderig's approach [43].
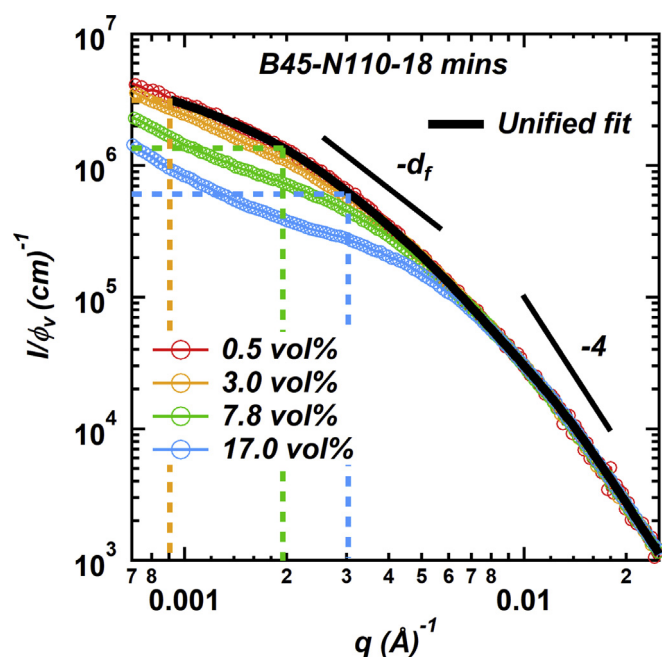
Fig. 5. Concentration dependence for the volume fraction normalized scattering intensities vs q for B45-N110 nanocomposite milled for 18 min; the high q regions ($q > 0.01$) overlap but there is a decrease in the reduced intensity in the low q range ($0.001 < q < 0.01$) indicating screening of the aggregates. The horizontal lines are values for $\frac{1}{\nu\phi_v}$ obtained from the fits, a measure of the drop in reduced intensity due to structural screening. The vertical lines from the intersection of $\frac{1}{\nu\phi_v}$ and dilute (0.5 vol percent) curve is a measure of the local network mesh size $\xi \approx 2\pi/q^*$; similar variation in scattering intensity with concentration for B54-N110 nanocomposite milled for 12 min is shown in Fig. S2 in the supplemental material.

dimension, $d_f \sim 1.8$, and connective dimension, $c \sim 1.2$, determined from the scattering parameters approximately agreed with those of the simulated structure following the code provided by Mulderig et al. [43]. The aggregate structures shown in Fig. 4 (c) and 4 (d), simulated with $z = 21$ and sticking probability of 0.45 reproduced similar mass-fractal parameters in subsequent simulations so that a family of 3d "average" aggregates matching the scattering results could be produced. These simulated 3d aggregates, can be used in DPD (dissipative particle dynamics) simulations for a deeper understanding of the effect of processing on the emergent nanocomposite structure.

3.2. Quantification of filler dispersion through screening

Fig. 5 shows the scattering profiles for B45-N110 nanocomposites milled for 18 min at different filler concentrations. The scattering intensities have been normalized with the volume fractions of the filler. The volume fraction was determined from the weight fraction such that $\phi_v = \frac{\rho_p}{\rho_p + \left(1 - \phi_{wt}/\phi_{wt}\right)\rho_f}$, where ρ_p is the density of the elastomer. At high q, ($q > 0.01$) the reduced scattering curves for all concentrations overlap in the primary particle regime. This indicates that increasing filler concentration does not affect the scattering from primary particles. However, at lower q's ($0.001 < q < 0.01$), a noticeable drop in normalized intensity is observed at all concentrations higher than the dilute condition. Consequently, the size and structure of the aggregate cannot be resolved. This is expected due to the increase in number of filler aggregates within the scattering volume. This reduction in normalized intensity is accounted for by the term $\nu\phi_v$ per equation (6). $\nu\phi_v$ is obtained by fitting the high concentration curves with the two-level Unified Fit parameters listed in Table S1 in the supplemental material such that a distinct value of $\nu\phi_v$ results at each concentration. The

screening parameter, ν is obtained from the linear dependence of $\nu\phi_v$ with the filler volume fraction ϕ_v. The diminution in reduced intensity of the nanocomposite characterized by ν is related to the pseudo-second virial coefficient (pseudo-A_2) through equation (7). Here, the contrast, $\langle\Delta\rho^2\rangle$ is the squared difference in electron densities between carbon black and elastomer. $\langle\Delta\rho^2\rangle$ is $59.4 \times 10^{20}\,\mathrm{cm}^{-4}$ for butadiene rubbers (B38, B45, B54). For styrene-butadiene rubbers, $\langle\Delta\rho^2\rangle$ is $55.4 \times 10^{20}\,\mathrm{cm}^{-4}$ (SB80-38, SB50-38) and $52.6 \times 10^{20}\,\mathrm{cm}^{-4}$ (SB50-26, SB62-26).

3.3. The kinetics of mixing and time-temperature analogy

The mixing of fillers such as carbon black in elastomers and the subsequent dispersion and distribution of filler aggregates depends on the accumulated strain. At a constant rate of shear, longer mixing times results in larger accumulated shear strain [50]. Fig. 6(a) shows the variation in pseudo-A_2 normalized by $\frac{M^2}{N_A}$ as a function of inverse mixing time, $\frac{1}{t}$ (in analogy to thermal energy, $1/k_B T$), equation (9), for B45-N110 and B54-N110 nanocomposites. Similar plots for N110 filled SB80-38 and SB50-38 are shown in Fig. 6(b); for SB50-26 and SB62-26 are shown in Fig. 6(c). The styrene-butadiene rubbers were grouped based on weight percent styrene content as detailed in Table 1. From Fig. 6 (a)-(c), it is observed that an increase in t, i.e. a reduction in $1/t$, is marked by an increase in A_2 indicating better dispersion. Similar temperature dependent behavior has been observed in thermally-dispersed colloidal solutions [51], that is better dispersion at higher temperatures. This indicates that dispersion improves with mixing time as expected, and in a manner analogous to temperature in a thermally-dispersed colloidal dispersion. This increase is also similar to the improvement in dispersion rating with increasing mixing time reported in the literature [9,10]. However, there is an upper limit to this dispersion such that there exists a terminal state of dispersion. This terminal state of dispersion is also observed in macro-dispersion studies [9,12] at very long mixing times.

The dependence of the pseudo-A_2 on the filler type is shown in Fig. 6(d). It is seen that for all mixing times, the pseudo-A_2 is larger for N330 carbon black aggregates than N110 carbon black aggregates. This indicates that it is easier to disperse larger nanoparticles and that the influence of accumulated strain is larger on the larger nanoparticles [26]. This could be because a larger particle displays a larger lever arm under similar shear stress resulting in a larger applied force. The opposite dependence on particle size is observed in thermally-dispersed colloids where smaller nanoparticles are more easily dispersed by thermal motion [34].

Positive values of pseudo-A_2 indicate miscibility in a thermally-dispersed colloid due to repulsive forces between the particles. Generally, an increase in the temperature results in an increase in A_2 for solutions that display an upper critical solution temperature. The pseudo-A_2 is a measure of dispersion in kinetically-dispersed colloids. Positive pseudo-A_2 indicates a dispersed system while negative pseudo-A_2 indicates flocculation or coagulation of the filler.

The filler/elastomer mixture displays net attractive forces between the nanoparticles that are opposed by the accumulated shear strain. Even at low concentrations we expect significant clustering of the nanoparticles so that the overlap concentration as normally calculated is not an appropriate measure of the point in concentration where global percolation occurs. The traditional overlap concentration can be estimated in volume fraction by $\phi^* = z\left(\frac{d_p}{R_{eted}}\right)^3$. This has a value of about $\phi^* \approx 0.4$ for the nanocomposites listed in Table 3. This value is close to the observed value for carbon black bulk percolation using conductivity measurements. In scattering we observe significant interaction between particles that leads to screening above about $\phi \approx 0.03$. This can be considered as the point where the attractive interactions lead to clustering of the nanoparticles, and associated screening of scattering, which is opposed by the accumulated shear strain. The filler/elastomer
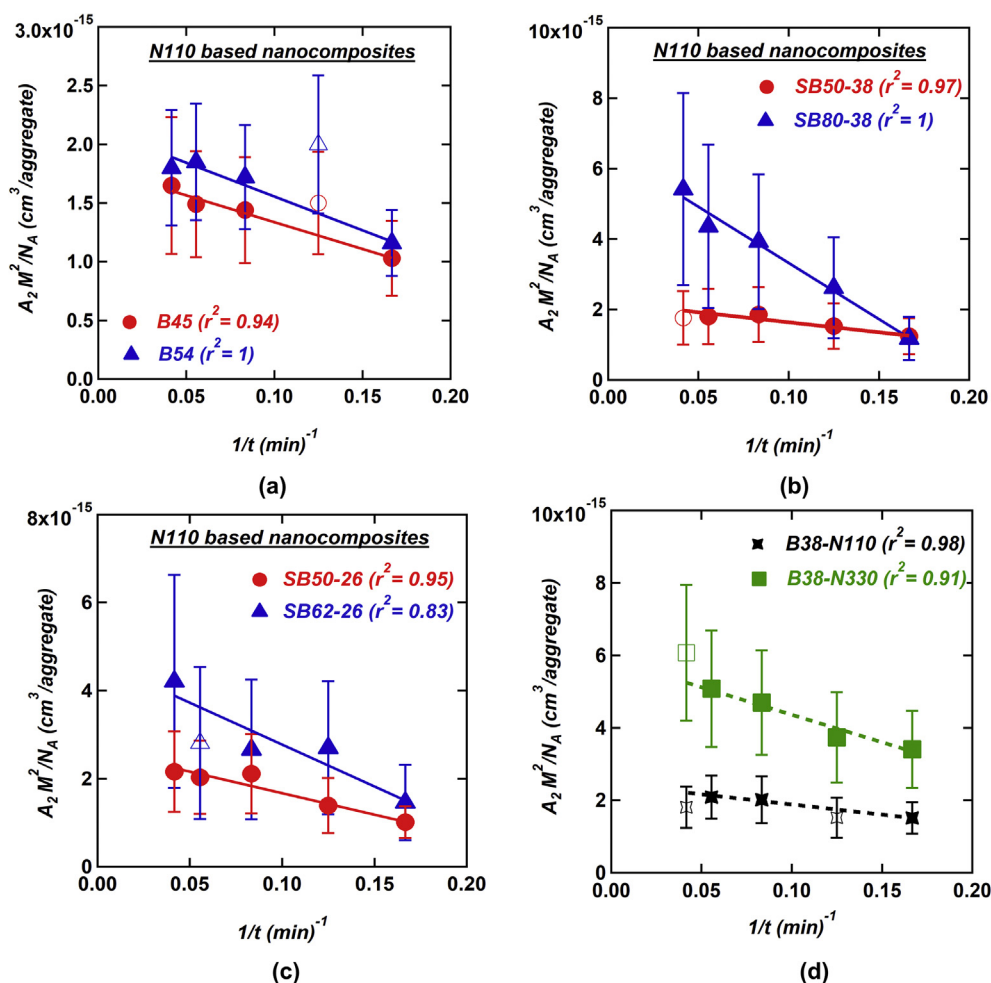
Fig. 6. Pseudo-A_2 normalized by $\frac{M^2}{N_A}$ following equation (9) vs $1/t$ for N110 based (a) B45, B54; (b) SB80-38, SB50-38; (c) SB50-26, SB62-26 nanocomposites; (d) comparison between B38-N110 (filled black stars) and B38-N330 (filled green squares); for similar curves with N330 carbon black refer to Fig. S3 in the supplemental material. Note all fits are error weighted; all outliers (indicated by open symbols) are excluded from the fits. (For interpretation of the references to colour in this figure legend, the reader is referred to the Web version of this article.)

Table 3
Pseudo-van der Waals parameters a^* and b^* obtained by fitting equation (9) to the data points in Fig. 6 for N110 based nanocomposites and data points in Fig. S3 in the supplemental material for N330 based nanocomposites. (Extra significant figures are included in some cases since the reported error is possibly an over estimation.)

Elastomer	Carbon black	$a^* \times 10^{-15}$ (cm³min/aggregate)	$b^* \times 10^{-15}$ (cm³/aggregate)
B38	N110	6 ± 6	2.4 ± 0.8
B45		5 ± 4	1.8 ± 0.5
B54		6 ± 4	2.1 ± 0.5
SB80-38		32 ± 14	6.5 ± 2
SB50-38		6 ± 8	2.2 ± 1
SB50-26		10 ± 6	2.7 ± 0.8
SB62-26		19 ± 16	4.7 ± 2
B38	N330	15 ± 15	5.9 ± 2
B45		3 ± 6	1.7 ± 0.7
B54		12 ± 12	3.6 ± 2
SB80-38		47 ± 27	10 ± 4
SB50-38		10 ± 10	3.2 ± 2
SB50-26		13 ± 10	4.1 ± 1
SB62-26		40 ± 40	12 ± 5

system displays two critical concentrations, one associated with percolation of agglomerates where bulk conductivity is expected at 20 to 40 vol percent, and one associated with local clustering and percolation

on the nanoscale of aggregates at about 3–5 vol percent where structural screening is observed in scattering and local clustering impacts the dynamic mechanical properties [29].

The curves in Fig. 6 are fit to the modified van der Waals equation, equation (9), and the parameters are listed in Table 3. The excluded volume term, b^* is measured in cm³/aggregate akin to thermally-dispersed colloidal solutions. However, the units of a^* (cm³min/aggregate) differ from a due to the time dependence proposed in this work.

Fig. 7 shows $V_{ex} = b^*/z$ or the excluded volume per primary particle for both N110 and N330 carbon black based nanocomposites. It is observed that for a given carbon black V_{ex} remains constant for all elastomer grades. This independence of V_{ex} from the chemical structure as well as the viscosity of the elastomer indicates that V_{ex} is an inherent property of each carbon black filler. This terminal state of dispersion (at infinite mixing time) can be envisioned as the complete breakdown of filler aggregates to their constituent primary particles. Under these circumstances, interparticle repulsion due to the excluded volume depends on the size of the primary particles.

From Fig. 7, it can be seen that V_{ex} for N330 particles is larger than N110 particles. This agrees with the primary particle size for the two carbon blacks which is larger for N330. The excluded volume for a pair of hard spheres is expected to be four times the volume of the sphere. Since the primary particle size remains unchanged with elastomer type and mixing time, this model can be used by considering the hard sphere diameter to be equal to the average d_p over different nanocomposites.
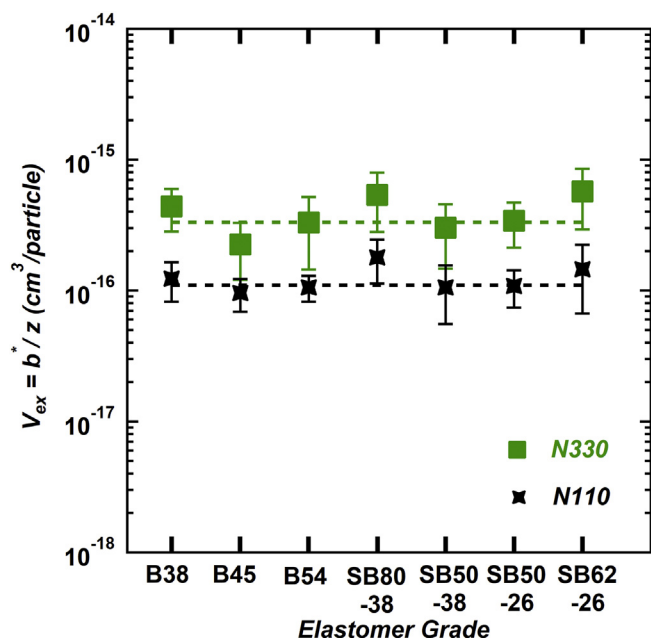
Fig. 7. Terminal state of dispersion characterized by the excluded volume b^* normalized by the degree of aggregation as a function of different elastomer grades for both carbon blacks – N110 (black stars) and N330 (green squares). The dashed horizontal lines indicate the average V_{ex} for each carbon black over all elastomer grades. (For interpretation of the references to colour in this figure legend, the reader is referred to the Web version of this article.)

For N110 the average d_p is about 28 nm resulting in a theoretical excluded volume of about 0.5×10^{-16} cm^3/particle. Similarly, an average d_p of 42 nm for N330 results in an excluded volume of about 1.5×10^{-16} cm^3/particle. The experimentally determined V_{ex} from Fig. 7, is 1 ($\pm$ 0.1) x 10^{-16} cm^3/particle and 3 ($\pm$ 0.6) x 10^{-16} cm^3/particle for N110 and N330 carbon blacks respectively. These excluded volume estimates for the primary particles are slightly larger than the theoretical hard sphere excluded volume. The effective diameter determined from the ratio of V_{ex} to the hard sphere excluded volume, V_{ex}^{HS} is $\sim 1.3 d_p$ for both carbon blacks. For an aggregate comprised of 'z' fused primary particles, one would expect, the experimental excluded volume to be smaller than the theoretical on purely geometrical arguments [52]. However, the above estimate confirms that the assumption of spherical primary particles is reasonable. It seems that shear flow does not affect the symmetry of these particles.

The excess excluded volume per primary particle, $V_{excess} = V_{ex} - V_{ex}^{HS}$ could be thought of as a consequence of the bound rubber layer in the nanocomposite. The primary bound rubber layer occupies a certain volume around the filler particles that is inaccessible to other filler particles [53] and is a consequence of favorable filler-polymer interactions [54]. The thickness of this layer determined from the excess excluded per particle is on the order of 5 nm for both carbon blacks. Unlike the bound rubber content determined from solvent extraction methods, which is a function of the specific surface area of the filler [55–57], matrix viscosity [58], mixing duration [3,11] and filler loading [55], the local bound layer thickness is expected to be a constant.

In contrast to V_{ex}, which does not vary with elastomer type, a^* varies with the type of elastomer such that a^* is larger for higher viscosities, thus higher viscosity retards dispersion. A larger value of a^* for higher viscosity elastomers with the same chemical structure, manifests as an increase in the time taken for filler incorporation prior to aggregate dispersion. This wetting time for the filler is termed the incorporation time based on kinetic studies on macro dispersion [12] and electrical conductivity [34,35]. Similar to the Boyle temperature defined at $A_2 = 0$, a characteristic time $t^* = a^*/b^*$ can be defined where the polymer chains have not penetrated into the carbon black agglomerates. Fig. 8 shows this characteristic time as a function of elastomer viscosity for carbon black containing nanocomposites. Since b^* is a property of the filler, t^* for a given filler type only depends on a^* which increases with viscosity. Viscosity is related to the molecular weight of the elastomer, typically it is observed at high molecular weight that $\eta \sim M^{3.4}$. An increase in matrix viscosity means there are longer molecular chains that have more entanglements. This implies a longer time is required for diffusion of polymer chains into the carbon black structure. Following the reptation theory [59], the relaxation time for polymer self-diffusion is directly proportional to the cube of polymer molecular weight, $\tau \sim M^3$. Combining these two expressions leads to $\tau \sim \eta^{0.9}$ or a near linear dependence between viscosity and relaxation time which agrees with the dependence seen in Fig. 8. This implies that a high viscosity matrix delays filler incorporation.

Alternatively, it can be considered that wetting occurs at a fixed value of accumulated strain, $\langle \gamma \rangle^*$. Viscosity is defined as the stress divided by the rate of strain, $\eta \sim \tau/\dot{\gamma}$. If wetting occurs at a fixed accumulated strain, $\langle \gamma \rangle^* = t^* \langle \dot{\gamma} \rangle$, then it is expected that the wetting time, t^*, will be proportional to the viscosity, $t^* = \langle \gamma \rangle^* / \langle \dot{\gamma} \rangle = \eta \langle \gamma \rangle^* / \tau$ which is observed in Fig. 8.

Interestingly, Fig. 8(a) and (b) show similar wetting times of ~ 3 min for N110 as well as N330 carbon blacks loaded in SB50-38 (solid green square) and SB50-26 (solid/open blue triangle). These
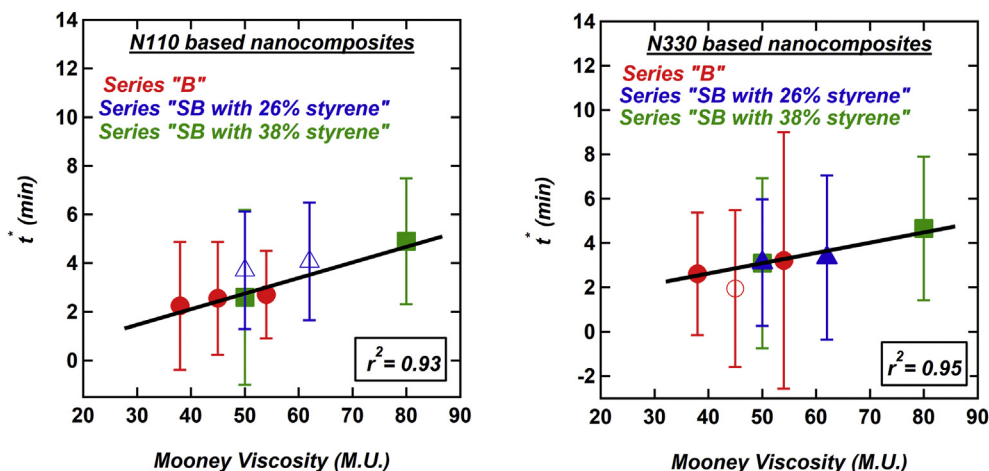
Fig. 8. Characteristic incorporation time, t^* for N110 (a) and N330 (b) carbon black based nanocomposites with different Mooney viscosities. Note that the filler was added after 1 min of commencement of the mixing operation. All fits are error weighted and open symbols are excluded from the fits.

elastomers have the same Mooney viscosity of 50 M U. but different styrene content by weight. The interaction of carbon black with butadiene units was found to be stronger than with styrene units by Choi [60]. This means that for the same matrix viscosity, an elastomer with larger styrene content would impede carbon black incorporation. The results shown in Fig. 8(a) and (b) do not support this for nanoscale mixing, although the propagated error bars could mask this behavior.

Fig. 8(a) and 8(b), also compare the wetting time as a function of particle size. Cotton estimated that carbon blacks with a lower oil absorption number (OAN) incorporate into the matrix faster [61]. The OAN for N330 is 102 ml/100g whereas it is 113 ml/100g for N110 [46]. Cotton's estimate is indistinguishable from this result since the wetting times for both carbon fillers are comparable under different matrix viscosities. Additionally, the intercept to the trendlines is close to 0, indicating that for low viscosity systems such as printing inks, the colloidal particles incorporate into the matrix readily.

Nano-dispersion quantified by A_2 above, can be modelled through a simple van der Waals approach by considering an analogy between thermal energy in thermally-dispersed colloidal systems and mixing kinetics in highly viscous, kinetically-dispersed, industrial nanofilled systems driven by accumulated strain. Although, some prior work on nanoparticle stability in liquid to polymeric matrices has been tested, [62] the processing history of the samples is generally overlooked. The proposed quantification of dispersion via scattering is not limited to local measurements as in the case of micrograph analysis. This model also parallels the determination of filler incorporation time from online conductivity and torque measurements. A measure of pseudo-A_2 from the fractal aggregates as proposed in this method could also aid the well-established simulation methods that generally assume spherical particles and binary interaction potentials [63]. In terms of SAXS and SANS, the quantification of dispersion, more often than not, focuses on colloidal/precipitated silica which correlate strongly on the aggregate level [64,65]. Although the proposed method takes advantage of a mean-field approach to quantify pseudo-A_2 for weakly correlating carbon blacks, it can be extended to these strongly correlated systems [66]. The proposed thermal-dispersion model attempts to relate the processing conditions to the nanoparticle dispersion in kinetically dispersed systems. Of the two parameters in the model, the excluded volume term depends only on the size of the primary particles. The description of excess excluded volume is consistent with the local bound rubber layer thickness. The pseudo-interaction term depends on the matrix viscosity and is directly related to the filler wetting time.

4. Conclusions

Through an analogy with thermally dispersed colloids an analysis is made of the mixing time dependence of dispersion in reinforced elastomers for two carbon blacks and elastomers with variable chemistry and viscosity. It is found that a simple use of a modified van der Waals equation for the second virial coefficient can account for the time dependence of mixing. The excluded volume term does not depend on matrix type or viscosity but strongly depends on the size of the carbon black particles. The excess excluded volume is determined to be a constant which seems consistent with the description of the bound rubber layer in mixing of carbon black with elastomers on the nanoscale. Contrary to this independence of the excluded volume on matrix type, it is found that the pseudo-interaction term strongly depends on viscosity and a plausibly weak dependence on chemical interactions of the elastomer and filler. These findings are consistent with a direct analogy between mixing time and accumulated strain with temperature for thermally-dispersed colloidal systems. The thermal-dispersion analogy allows calculation of the wetting time for carbon black, which is proportional to the elastomer viscosity as might be expected from reptation theory or from a simple estimate of the accumulated strain. The thermal-dispersion analogy for kinetically-dispersed colloids offers a new understanding and parameterization of

dispersion in nanocomposites and the potential for predictive capabilities.

Based on the thermal-dispersion model, presented in this paper, the impact of kinetic energy is top-down while the impact of thermal energy is bottom-up. This combined with clustering of thermally immiscible nanoparticles lead to a complex hierarchy of structure compared to the relatively simple structural dispersion in thermally dispersed colloids. For nano-reinforced elastomers it is this hierarchy that serendipitously leads to the rich and complex mechanical and dynamic properties observed in commercial reinforced elastomers.

Notes

The authors declare no competing financial interest.

Appendix A. Supplementary data

Supplementary data to this article can be found online at https://doi.org/10.1016/j.polymer.2019.03.044.

References

[1] G.R. Cotten, Mixing of carbon black with rubber I. Measurement of dispersion rate by changes in mixing torque, Rubber Chem. Technol. 57 (1984) 118–133, https://doi.org/10.5254/1.3535988.

[2] H. Kondo, Evaluation of rubber processing for unvulcanized rubber, Nippon Gomu Kyokaishi 87 (2014) 16–21, https://doi.org/10.2324/gomu.87.16.

[3] G.R. Cotten, Mixing of carbon black with rubber IV. Effect of carbon black characteristics, Plast. Rubber Process. Appl. 7 (1987) 173–178.

[4] S. Shiga, M. Furuta, Processability of EPR in an internal mixer (II) morphological changes of carbon black agglomerates during mixing, Nippon Gomu Kyokaishi 55 (1982) 491–503, https://doi.org/10.2324/gomu.55.491.

[5] P. Raut, N. Swanson, A. Kulkarni, C. Pugh, S.C. Jana, Exploiting arene-perfluoroarene interactions for dispersion of carbon black in rubber compounds, Polymers 148 (2018) 247–258, https://doi.org/10.1016/j.polymer.2018.06.025.

[6] T. Mondal, A.K. Bhowmick, R. Ghosal, R. Mukhopadhyay, Expanded graphite as an agent towards controlling the dispersion of carbon black in poly (styrene –co-butadiene) matrix: an effective strategy towards the development of high performance multifunctional composite, Polymers 146 (2018) 31–41, https://doi.org/10.1016/j.polymer.2018.05.031.

[7] C.H. Leigh-Dugmore, Measurement of dispersion in black-loaded rubber, Rubber Chem. Technol. 29 (1956) 1303–1308, https://doi.org/10.5254/1.3542632.

[8] A.I. Medalia, Dispersion of carbon black in rubber: revised calculation procedure, Rubber Chem. Technol. 34 (1961) 1134–1140, https://doi.org/10.5254/1.3540272.

[9] A.Y. Coran, J.-B. Donnet, The dispersion of carbon black in rubber Part I. Rapid method for assessing quality of dispersion, Rubber Chem. Technol. 65 (1992) 973–997, https://doi.org/10.5254/1.3538655.

[10] A.Y. Coran, J. Donnet, The dispersion of carbon black in rubber Part II. The kinetics of dispersion in natural rubber, Rubber Chem. Technol. 65 (1992) 998–1015, https://doi.org/10.5254/1.3538656.

[11] J. Leblanc, Rubber–filler interactions and rheological properties in filled compounds, Prog. Polym. Sci. 27 (2002) 627–687, https://doi.org/10.1016/S0079-6700(01)00040-5.

[12] A.Y. Coran, F. Ignatz-Hoover, P.C. Smakula, The dispersion of carbon black in rubber Part IV. The kinetics of carbon black dispersion in various polymers, Rubber Chem. Technol. 67 (1994) 237–251, https://doi.org/10.5254/1.3538671.

[13] H.H. Le, E. Hamann, S. Ilisch, G. Heinrich, H.J. Radusch, Selective wetting and dispersion of filler in rubber composites under influence of processing and curing additives, Polymers 55 (2014) 1560–1569, https://doi.org/10.1016/j.polymer.2014.02.002.

[14] F. Faraguna, P. Pötschke, J. Pionteck, Preparation of polystyrene nanocomposites

with functionalized carbon nanotubes by melt and solution mixing: investigation of dispersion, melt rheology, electrical and thermal properties, Polymers 132 (2017) 325–341, https://doi.org/10.1016/j.polymer.2017.11.014.

[15] F. Bohin, D.L. Feke, I. Manas-Zloczower, Analysis of power requirements and dispersion quality in batch compounding using a dispersion model for single agglomerates, Rubber Chem. Technol. 69 (1996) 1–7, https://doi.org/10.5254/1.3538355.

[16] H. Yamada, I. Manas-Zloczower, D.L. Feke, The influence of matrix viscosity and interfacial properties on the dispersion kinetics of carbon black agglomerates, Rubber Chem. Technol. 71 (1998) 1–16, https://doi.org/10.5254/1.3538468.

[17] B. Lively, P. Smith, W. Wood, R. Maguire, W.H. Zhong, Quantified stereological macrodispersion analysis of polymer nanocomposites, Compos. Part A Appl. Sci. Manuf. 43 (2012) 847–855, https://doi.org/10.1016/j.compositesa.2012.01.012.

[18] H.S. Khare, D.L. Burris, A quantitative method for measuring nanocomposite dispersion, Polymer 51 (2010) 719–729, https://doi.org/10.1016/j.polymer.2009.12.031.

[19] Z. Li, Y. Gao, K.-S. Moon, Y. Yao, A. Tannenbaum, C.P. Wong, Automatic quantification of filler dispersion in polymer composites, Polymer 53 (2012) 1571–1580, https://doi.org/10.1016/j.polymer.2012.01.048.

[20] T. Glaskova, M. Zarrelli, A. Aniskevich, M. Giordano, L. Trinkler, B. Berzina, Quantitative optical analysis of filler dispersion degree in MWCNT-epoxy nanocomposite, Compos. Sci. Technol. 72 (2012) 477–481, https://doi.org/10.1016/j.compscitech.2011.11.029.

[21] T. Glaskova, M. Zarrelli, A. Borisova, K. Timchenko, A. Aniskevich, M. Giordano, Method of quantitative analysis of filler dispersion in composite systems with spherical inclusions, Compos. Sci. Technol. 71 (2011) 1543–1549, https://doi.org/10.1016/j.compscitech.2011.06.009.

[22] M.D. Haslam, B. Raeymaekers, A composite index to quantify dispersion of carbon nanotubes in polymer-based composite materials, Compos. B Eng. 55 (2013) 16–21, https://doi.org/10.1016/j.compositesb.2013.05.038.

[23] X. Fu, J. Wang, J. Ding, H. Wu, Y. Dong, Y. Fu, Quantitative evaluation of carbon nanotube dispersion through scanning electron microscopy images, Compos. Sci. Technol. 87 (2013) 170–173, https://doi.org/10.1016/j.compscitech.2013.08.014.

[24] S.R. Bakshi, R.G. Batista, A. Agarwal, Quantification of carbon nanotube distribution and property correlation in nanocomposites, Compos. Part A Appl. Sci. Manuf. 40 (2009) 1311–1318, https://doi.org/10.1016/j.compositesa.2009.06.004.

[25] S. Pegel, P. Pötschke, T. Villmow, D. Stoyan, G. Heinrich, Spatial statistics of carbon nanotube polymer composites, Polymer 50 (2009) 2123–2132, https://doi.org/10.1016/j.polymer.2009.02.030.

[26] D.J. Bray, S.G. Gilmour, F.J. Guild, A.C. Taylor, Quantifying nanoparticle dispersion by using the area disorder of Delaunay triangulation, J. R. Stat. Soc. Ser. C Appl. Stat. 61 (2012) 253–275, https://doi.org/10.1111/j.1467-9876.2011.01009.x.

[27] R. Krishnamoorti, Strategies for dispersing nanoparticles in polymers, MRS Bull. 32 (2007) 341–347, https://doi.org/10.1557/mrs2007.233.

[28] Y. Jin, G. Beaucage, K. Vogtt, H. Jiang, V. Kuppa, J. Kim, J. Ilavsky, M. Rackaitis, A. Mulderig, K. Rishi, V. Narayanan, A pseudo-thermodynamic description of dispersion for nanocomposites, Polymer 129 (2017) 32–43, https://doi.org/10.1016/j.polymer.2017.09.040.

[29] K. Rishi, G. Beaucage, V. Kuppa, A. Mulderig, V. Narayanan, A. McGlasson, M. Rackaitis, J. Ilavsky, Impact of an emergent hierarchical filler network on nanocomposite dynamics, Macromolecules 51 (2018) 7893–7904, https://doi.org/10.1021/acs.macromol.8b01510.

[30] K.W. Stöckelhuber, A. Das, R. Jurk, G. Heinrich, Contribution of physico-chemical properties of interfaces on dispersibility, adhesion and flocculation of filler particles in rubber, Polymer 51 (2010) 1954–1963, https://doi.org/10.1016/j.polymer.2010.03.013.

[31] I. Hassinger, X. Li, H. Zhao, H. Xu, Y. Huang, A. Prasad, L. Schadler, W. Chen, L. Catherine Brinson, Toward the development of a quantitative tool for predicting dispersion of nanocomposites under non-equilibrium processing conditions, J. Mater. Sci. 51 (2016) 4238–4249, https://doi.org/10.1007/s10853-015-9698-1.

[32] B. Natarajan, Y. Li, H. Deng, L.C. Brinson, L.S. Schadler, Effect of interfacial energetics on dispersion and glass transition temperature in polymer nanocomposites, Macromolecules 46 (2013) 2833–2841, https://doi.org/10.1021/ma302281b.

[33] C.P. O'Farrell, M. Gerspacher, L. Nikiel, Carbon black dispersion by electrical measurements, KGK - Kautsch. Gummi Kunstst. 53 (2000) 701–710.

[34] H.H. Le, S. Ilisch, B. Jakob, H. Radusch, Online characterization of the effect of mixing parameters on carbon black dispersion in rubber compounds using electrical conductivity, Rubber Chem. Technol. 77 (2004) 147–160, https://doi.org/10.5254/1.3547808.

[35] H.H. Le, M. Tiwari, S. Ilisch, H.J. Radusch, Effect of molecular structure on carbon black dispersion in rubber compounds, Kautsch. Gummi Kunstst. (2005) 575–580.

[36] A. Mulderig, G. Beaucage, K. Vogtt, H. Jiang, Y. Jin, L. Clapp, D.C. Henderson, Structural emergence in particle dispersions, Langmuir 33 (2017) 14029–14037, https://doi.org/10.1021/acs.langmuir.7b03033.

[37] F. Bonneté, S. Finet, A. Tardieu, Second virial coefficient: variations with lysozyme crystallization conditions, J. Cryst. Growth 196 (1999) 403–414, https://doi.org/10.1016/S0022-0248(98)00826-4.

[38] M. Takenaka, Analysis of structures of rubber-filler systems with combined scattering methods, Polym. J. 45 (2013) 10–19, https://doi.org/10.1038/pj.2012.187.

[39] G. Beaucage, H.K. Kammler, S.E. Pratsinis, Particle size distributions from small-angle scattering using global scattering functions, J. Appl. Crystallogr. 37 (2004) 523–535, https://doi.org/10.1107/S0021889804008969.

[40] G. Beaucage, Determination of branch fraction and minimum dimension of mass-fractal aggregates, Phys. Rev. E. 70 (2004) 031401, https://doi.org/10.1103/PhysRevE.70.031401.

[41] G. Beaucage, Approximations leading to a unified exponential/power-law approach to small-angle scattering, J. Appl. Crystallogr. 28 (1995) 717–728, https://doi.org/10.1107/S0021889895005292.

[42] T. Koga, M. Takenaka, K. Aizawa, M. Nakamura, T. Hashimoto, Structure factors of dispersible units of carbon black filler in rubbers, Langmuir 21 (2005) 11409–11413, https://doi.org/10.1021/la051352s.

[43] A. Mulderig, G. Beaucage, K. Vogtt, H. Jiang, V. Kuppa, Quantification of branching in fumed silica, J. Aerosol Sci. 109 (2017) 28–37, https://doi.org/10.1016/j.jaerosci.2017.04.001.

[44] K. Vogtt, G. Beaucage, M. Weaver, H. Jiang, Thermodynamic stability of worm-like micelle solutions, Soft Matter 13 (2017) 6068–6078, https://doi.org/10.1039/C7SM01132F.

[45] S. Ceccia, F. Bellucci, O. Monticelli, A. Frache, G. Traverso, A. Casale, The effect of annealing conditions on the intercalation and exfoliation of layered silicates in polymer nanocomposites, J. Polym. Sci., Part B: Polym. Phys. 48 (2010) 2476–2483, https://doi.org/10.1002/polb.22146.

[46] Reinforcing carbon blacks, n.d. http://www.cabotcorp.com/solutions/products-plus/carbon-blacks-for-elastomer-reinforcement/reinforcing , Accessed date: 16 July 2018.

[47] J. Ilavsky, P.R. Jemian, A.J. Allen, F. Zhang, L.E. Levine, G.G. Long, Ultra-small-angle X-ray scattering at the advanced Photon Source, J. Appl. Crystallogr. 42 (2009) 469–479, https://doi.org/10.1107/S0021889809008802.

[48] E. Hoinkis, E.B.F. Lima, P. Schubert-Bischoff, A study of carbon black corax N330 with small-angle scattering of neutrons and X-rays, Langmuir 20 (2004) 8823–8830, https://doi.org/10.1021/la0302596.

[49] M.-J. Wang, S. Wolff, E.-H. Tan, Filler-elastomer interactions. Part VIII. The role of the distance between filler aggregates in the dynamic properties of filled vulcanizates, Rubber Chem. Technol. 66 (1993) 178–195, https://doi.org/10.5254/1.3538305.

[50] Z. Tadmor, C.G. Gogos, Principles of Polymer Processing, second ed., John Wiley & Sons, Inc., Hoboken, NJ, USA, 2006.

[51] K. Rishi, A. Mulderig, G. Beaucage, K. Vogtt, H. Jiang, L. Clapp, D.C. Henderson, Thermodynamics of Hierarchical Aggregation in Pigment Dispersions, n.d.

[52] Trokhymchuk, Nezbeda Melnyk, Virial expansions and augmented van der Waals approach: application to Lennard-Jones-like Yukawa fluid, Condens. Matter Phys. 18 (2015) 13501, https://doi.org/10.5488/CMP.18.13501.

[53] S.S. Choi, E. Ko, Novel test method to estimate bound rubber formation of silica-filled solution styrene-butadiene rubber compounds, Polym. Test. 40 (2014) 170–177, https://doi.org/10.1016/j.polymertesting.2014.09.003.

[54] J. Liu, H. Wan, H. Zhou, Y. Feng, L. Zhang, A.V. Lyulin, Formation mechanism of bound rubber in elastomer nanocomposites: a molecular dynamics simulation study, RSC Adv. 8 (2018) 13008–13017, https://doi.org/10.1039/c8ra00405f.

[55] C.G. Robertson, C.J. Lin, M. Rackaitis, C.M. Roland, Influence of particle size and Polymer−Filler coupling on viscoelastic glass transition of particle-reinforced polymers, Macromolecules 41 (2008) 2727–2731, https://doi.org/10.1021/ma7022364.

[56] S. Wolff, M.-J. Wang, E.-H. Tan, Filler-elastomer interactions. Part VII. Study on bound rubber, Rubber Chem. Technol. 66 (1993) 163–177, https://doi.org/10.5254/1.3538304.

[57] B. Meissner, Bound rubber and elastomer-filler interaction, Rubber Chem. Technol. 68 (1995) 297–310, https://doi.org/10.5254/1.3538744.

[58] J. Duke, W.K. Taft, I.M. Kolthoff, Formation of bound rubber of GR-S type polymers with carbon blacks, Ind. Eng. Chem. 43 (1951) 2885–2892, https://doi.org/10.1021/ie50504a063.

[59] M. Doi, S.F. Edwards, The Theory of Polymer Dynamics, Oxford university press, 1988.

[60] S.-S. Choi, Filler-polymer interactions in both silica and carbon black-filled styrene-butadiene rubber compounds, J. Polym. Sci., Part B: Polym. Phys. 39 (2001) 439–445, https://doi.org/10.1002/1099-0488(20010215)39:4 < 439::AID-POLB1016 > 3.0.CO;2-3.

[61] G.R. Cotten, Mixing of carbon black with rubber. II. Mechanism of carbon black incorporation, Rubber Chem. Technol. 58 (1985) 774–784, https://doi.org/10.5254/1.3536092.

[62] B.J. Anderson, C.F. Zukoski, Nanoparticle stability in polymer melts as determined by particle second virial measurement, Macromolecules 40 (2007) 5133–5140, https://doi.org/10.1021/ma0624346.

[63] J. Liu, Y. Gao, D. Cao, L. Zhang, Z. Guo, Nanoparticle dispersion and aggregation in polymer nanocomposites: insights from molecular dynamics simulation, Langmuir 27 (2011) 7926–7933, https://doi.org/10.1021/la201073m.

[64] S. Kim, K. Hyun, B. Struth, K.H. Ahn, C. Clasen, Structural development of nanoparticle dispersion during drying in polymer nanocomposite films, Macromolecules 49 (2016) 9068–9079, https://doi.org/10.1021/acs.macromol.6b01939.

[65] N. Gundlach, R. Hentschke, Modelling filler dispersion in elastomers: relating filler morphology to interface free energies via SAXS and TEM simulation studies, Polymers 10 (2018) 446, https://doi.org/10.3390/polym10040446.

[66] A. McGlasson, G. Beaucage, M. Chauby, K. Rishi, V. Kuppa, J. Ilavsky, Quantification of Dispersion in Polymer Nanocomposites for Weakly and Strongly Correlated Nanofillers, n.d.